Since January 2020 Elsevier has created a COVID-19 resource centre with free information in English and Mandarin on the novel coronavirus COVID-19. The COVID-19 resource centre is hosted on Elsevier Connect, the company's public news and information website.

International Journal of Biological Macromolecules xxx (xxxx) xxx

Contents lists available at ScienceDirect

International Journal of Biological Macromolecules

journal homepage: www.elsevier.com/locate/ijbiomac

The inhibitory activity of methoxyl flavonoids derived from *Inula britannica* flowers on SARS-CoV-2 3CLpro

Jang Hoon Kim [a,1], Yea-In Park [b,1], Mok Hur [a], Woo Tae Park [a], Youn-Ho Moon [a], Sung Cheol Koo [a], Yun-Chan Her[a], Ik Soo Lee [c,*], Junsoo Park [b,*]

[a] Department of Herbal Crop Research, National Institute of Horticultural & Herbal Science, RDA, Eumsung 27709, Republic of Korea
[b] Division of Biological Science and Technology, Yonsei University, Wonju 26493, Republic of Korea
[c] Km Covergence Research Division, Korea Institute of Oriental Medicien, Daejeon, Republic of Korea

ARTICLE INFO

Keywords:
Inula britannica
Methoxyl flavonoids
SARS-CoV-2
3CLpro
HCoV-OC43

ABSTRACT

In our ongoing efforts to identify effective natural antiviral agents, four methoxy flavonoids (**1**–**4**) were isolated from the *Inula britannica* flower extract. Their structures were elucidated using nuclear magnetic resonance. Flavonoids **1**–**4** exhibited inhibitory activity against SARS- CoV-2 3CLpro with IC_{50} values of 41.6 ± 2.5, 35.9 ± 0.9, 32.8 ± 1.2, and 96.6 ± 3.4 μM, respectively. Flavonoids **1**–**3** inhibited 3CLpro in a competitive manner. Based on molecular simulations, key amino acids that form hydrogen bond with inhibitor **3** were identified. Finally, we found that inhibitors (**1**–**3**) suppressed HCoV-OC43 coronavirus proliferation at micromole concentrations.

1. Introduction

The genus *Inula*, a perennial herb distributed mainly in Asia, Europe, and Africa, consists of approximately 100 species belonging to the Asteraceae family [1], and many of these species used as traditional herbal medicines throughout the world [2,3]. *Inula britannica* L. is one of the most commonly used plants in traditional Chinese medicine (TCM) and Kampo medicines [4]. Its flowers have been widely used to treat digestive disorders, bronchitis, and various types of inflammation [5]. Furthermore, they have been shown to possess diverse biological activities, including antimicrobial, hepatoprotective, antidiabetic, hypolipidemic, antitumor, and anti-inflammatory properties [6–11]. These properties have been linked to the presence of various bioactive substances in the flowers of *I. britannica*, and a literature survey indicates that sesquiterpene lactones are the predominant secondary metabolites found in the flowers of this plant [4]. Furthermore, a large number of flavonoids known to play an important role in enzyme inhibition, antioxidant, and cytotoxic activity have been identified [4].

Severe acute respiratory syndrome coronavirus 2 (SARS-CoV-2), which belongs the family *Coronaviridase*, is an enveloped positive-sense single-stranded RNA virus [12]. COVID-19 (Coronavirus disease 2019) is an infectious disease caused by the SAR-CoV-2, and its symptoms include fever, cough, and lymphopenia [13]. 3C-like protease (3CLpro) is one of enzymes in the replication of SARS-CoV-2 [14]. In the early stage of virus replication, a polypeptide chain of approximately 800 kDa is translated from viral RNA by the ribosome and divided into 16 non-structure proteins (nsp), 12 of which are induced by SARS-CoV-2 3CLpro. Of these, nsp 12–16 were typically associated with viral RNA synthesis, proofreading, and modification [15]. Therefore, SARS-CoV-2 3CLpro has been regarded as a target enzyme for suppressing the proliferation of SARS-CoV-2. Recently, studies have been conducted to search for SARS-CoV-2 3CLpro inhibitors for the treatment of COVID-19 from natural and synthetic compounds [16]. As the results, paxlovid was developed as a SARS-CoV-2 3CLpro inhibitor for treatment of SARS-CoV-2 disease 2019 (Covid-19) [17], as well as components derived from *Ginkgo biloba* leaves and from *Ampelopsis grossedentata* were revealed the inhibitory activities with IC_{50} values within micromole concentration toward SARS-CoV-2 3CLpro [18,19].

In our ongoing efforts to identify effective natural antiviral agents, we found that four methoxy flavonoids (hispidulin, patuletin, nepetin, and isorhametin-3-*O*-glucoside), isolated from the *I. britannica* flower extract, exhibited considerable inhibitory effects on SARS-CoV-2 3CLpro enzymatic activity. Through the enzyme kinetic study, we confirmed binding of the inhibitor and SARS-CoV-2 3CLpro, and visually traced

* Corresponding authors.
E-mail addresses: knifer48@kiom.re.kr (I.S. Lee), junsoo@yonsei.ac.kr (J. Park).
[1] These authors contributed equally to this work.

https://doi.org/10.1016/j.ijbiomac.2022.10.008
Received 5 September 2022; Received in revised form 26 September 2022; Accepted 2 October 2022
Available online 5 October 2022

binding of the two, using molecular simulations. Finally, a cell-based HCoV-OC43 virus proliferation inhibition experiment was performed with methoxyl flavonoids.

2. Materials and methods

2.1. General experimental procedures

NMR experiments were conducted with a Bruker DRX-400 spectrometer (Bruker, Germany), with the chemical shift referenced to the residual solvent signals and using DMSO-d_6 as solvent. Thin-layer chromatography (TLC) analysis was performed on silica-gel 60 F254 and RP-18 F254S plates (both 0.25 mm layer thickness; Merck, Darmstadt, Germany). Compounds were visualized by dipping plates into 10 % (v/v) H_2SO_4 reagent, which were then air heat-treated at 300 °C for 15 s. Silica gel (60 A, 70–230 or 230–400 mesh ASTM; Merck) and reversed-phase silica gel (ODS-A 12 nm S-150, S-75 μm; YMC Co., Kyoto, Japan) were used for open column chromatography. SARS-CoV-2 3CLpro was purchased from Sigma Aldrich (St. Louis, MO, USA). DABCY-LKTSAVLQSGFRKME-EDANS was synthesized by Anygen (Gwangju, Korea).

2.2. Plant material

Flowers of *I. britannica* were purchased from a traditional herbal medicine store in Daejeon, Republic of Korea, in August 2020 and identified by Prof. Y.H. Kim (College of Pharmacy, Chungnam National University, Republic of Korea). A voucher specimen (IJ2020-030) has been deposited in the herbarium of the Korea Institute of Oriental Medicine, Republic of Korea.

2.3. Extraction and isolation

Air-dried flowers of *I. britannica* (200 g) were extracted in ethanol (2 L) at 80 °C for 3 h, filtered, and concentrated to yield an ethanol extract (10 g, 5 % yield). The extract was subjected to silica gel column chromatography (50 × 8.5 cm) using a methylene chloride–methanol (1:0 → 0:1) gradient solvent system. The column chromatographic fractions were combined to give four fractions (A, 1.2 g; B, 2.1 g; C, 3.2 g; D, 1.0) based on TLC data. Fraction B was subjected to RP-18 column chromatography (50 × 5 cm) using a methanol–water (20:80 → 90:10) gradient solvent system to yield four subfractions (B1–B4). Fraction B2 was further chromatographed on an RP-18 column (60 × 4 cm) using a methanol–water (60:40 → 80:20) gradient to afford compound **1** (25 mg). Fraction C was purified over an RP-18 column (50 × 5 cm) eluting with a methanol–water (20:80 → 90:10) gradient solvent system to generate four subfractions (C1–C4). Fraction C2 was further purified on an RP-18 column (60 × 4 cm) using a methanol–water (60:40 → 80:20) gradient to obtain compounds **2** (25 mg), **3** (28 mg), and **4** (32 mg).

2.4. 3CLpro inhibition assay

This assay was performed, as previously described, with modification [20]. 140 μL of 3CLpro (13.3 μg/mL) in 20 mM tris-HCl buffer (pH 7.5) was mixed in 10 μL of MeOH or compound in MeOH (12.5–200 μM) in a 96-well plate, and then 50 μL of 100 μM substrate were added. After starting each reaction at 37 °C, product was quantified using a fluorescence spectrophotometer set to measure 530 nm emission and 340 nm excitation with gain 85 during 30 min.

$$\text{Inhibitory activity rate } (\%) = [(\Delta C/\Delta S)/\Delta C] \times 100 \quad (1)$$

where ΔC and ΔS represent the intensity of control and inhibitor after 30 min, respectively.

$$y = y_0 + [(a \times x)/(b + x)] \quad (2)$$

where y_0 is the minimum value on the y-axis, a denotes the difference between maximum and minimum values, and b refers to the x value at 50 %.

2.5. Molecular docking

A three-dimensional (3D) structures of inhibitor were constructed and minimized using Chem3D Pro (CambridgeSoft, Cambridge, MA, USA). The 3D-structure of SARS CoV-2 3CLpro coded in 7END was downloaded from the RCSB protein data bank. Water and ligand (J7R) were then excluded from 3D-structure of enzyme. Hydrogen was added to the protein using AutoDockTools (Scripps Research, La Jolla, CA, USA); the Gasteiger charge model was then applied. Flexible ligand docking was achieved using a torsion tree, with detection of the torsion root and rotatable bonds. The grid box was set to a size of 60 × 60 × 60 at 0.375 Å for docking the ligand into the active site. Molecular docking was achieved via a Lamarckian genetic algorithm with the maximum number of evaluations. The resulting values were calculated and represented using Chimera 1.14 (San Francisco, CA, USA), and LIGPLOT (European Bioinformatics Institute, Hinxton, UK) [21].

2.6. Molecular dynamics

This research was performed as previously described [22]. The Gromacs version 4.6.5 package was used to simulate the complex of 3CLpro-methoxyl flavonoid. The complex was charged by a Gromos96 54a6 force field. Ligand topology was generated by The GlycoBioChem PRODRG2 Server. The charged complex was dissolved in water in a cubic box with a size of 10.5 × 10.5 × 10.5 using the simple point charge water model, and ionized with sodium. The mdp files were built following GROMACS instructions. They were minimized until a maximal force of 10 kJ/mol, using the steepest descent method. The product was further equilibrated by 300 K NVT in 1 bar NPT for 100 ps, respectively. Finally, a molecular dynamics simulation was conducted for 30 ns. The results were analyzed using g_utility. Generated data were visualized by Sigmaplot (San Jose, CA, USA) and chimera (San Francisco, CA, USA).

2.7. Plaque formation assay

Plaque formation assay was used to enumerate the coronavirus. RD cells were seeded in a 12-well plate one day prior to infection. The media containing coronavirus were diluted 10-fold in MEM (Welgene, Seoul, Korea) with 2 % Fetal Bovine Serum (FBS, Thermo Fisher Scientific, Waltham, MA, USA) and 1 % penicillin and streptomycin solution (Welgene). The diluted media were added to RD cells and incubated for 1 h at 33 °C and 5 % CO_2. Overlay medium containing 0.6 % agarose was added to each well and incubated for 3 days. After incubation, the cells were fixed with a 10 % formaldehyde solution and stained with 1 % crystal violet to visualize plaques. RD cells were obtained from Korean Cell Line Bank (KCLB, Seoul, Korea) and HCoV-OC43 was obtained from ATCC (Rockville, MD, USA).

2.8. Statistical analysis

All measurements were performed in triplicate across three independent experiments, and the results are shown as mean ± standard error of the mean (SEM). The results were analyzed using Sigma Plot (Systat Software Inc., San Jose, CS, USA).

3. Results

3.1. Isolation and identification of compounds 1–4

An ethanol extract of *I. britannica* flowers was subjected to silica gel column chromatography and divided into four fractions (A–D) based on

thin-layer chromatography (TLC) data. Flavonoid-rich fractions (B and C) were further subjected to a series of chromatographic separation steps, leading to the isolation of four yellowish compounds (**1**–**4**). Characteristic UV absorption maxima of these compounds suggested the presence of a flavonoid skeleton. Additional detailed comparison of ^{1}H and ^{13}C NMR data of these compounds with those in the literature identified four flavonoids, hispidulin (**1**) [23], patuletin (**2**) [23], nepetin (**3**) [2], and isorhametin-3-*O*-glucoside (**4**) [24] (Fig. 1).

3.2. The inhibitory activity of compounds *1*–*4* on SARS-CoV-2 3CLpro

Four flavonoids (**1**–**4**) were found to inhibit the catalytic reaction of SARS-CoV-2 3CLpro. As shown in Fig. 2, the flavonoids inhibited the production of DABCYL-KTSAVLQSGFRKME-EDANS into DABCYL-KTSAVLQ and SGFRKME-EDANS by the enzyme in a concentration-dependent manner. Their inhibitory rates were calculated by Eq. (1), and each inhibition rate at various concentrations induced Eq. (2). As a result, flavonoids **1**–**4** showed inhibitory activities with IC_{50} values of 42.0 ± 1.7, 34.0 ± 0.5, 31.7 ± 1.1, and 94.1 ± 2.5 μM, respectively (Fig. 2A and Table 1). Enzyme kinetics of the four flavonoids (**1**–**4**) with IC_{50} values under concentrations of 50 μM were performed to identify the binding position with SARS-CoV-2 3CLpro. The catalytic reaction of this and the substrate by the inhibitor within ~10 min was determined at the initial velocity (v_0). At each concentration, the inhibitor yielded a straight line induced by the various substrate concentrations. These results are shown in a Lineweaver–Burk plot. As indicated in Fig. 2B–D and Table 2, a linear equation of the four inhibitors had a y-axis (1/*V*max) value in common, and different x-axis (1/*K*m) values. Thus, these flavonoids act as the competitive inhibitors of SARS-CoV-2 3CLpro.

3.3. The prediction of binding sites between inhibitors and 3CLpro by molecular docking

The results of enzyme kinetics suggested that four inhibitors **1**–**3** bind to the active site of SARS-CoV-2 3CLpro. Molecular docking was performed to find the optimal binding site for enzymes and inhibitors. A grid (size 60 × 60 × 60) was set up to include all active sites for their expected binding sites. As indicated in Fig. 3A, inhibitors were stably fit to active site of 3CLpro. These inhibitors were calculated as autodock scores of −6.97, −7.2. and −7.17 kcal/mol, respectively (Table 2). Inhibitor **1** made respective five hydrogen bonds at 2.92, 2.90, 2.57, 3.13, and 2.74 Å distance with five amino acids (His164, Glu166, Arg188, Thr190, and Gln192) (Fig. 3B and Table 2). Also, inhibitor **2** kept five hydrogen bonds at 2.60, 2.58, 2.82, 2.98, and 2.73 Å distance with five amino acids (Glu166, Arg188, Gln189, Thr190, and Gln192). Finally, inhibitor **3** had seven hydrogen bonds at with Cys145 (2.85 Å), His164 (2.82 Å), Arg188 (3.03 Å), Thr190 (2.45, 2.91, and 2.93 Å), and Gln192 (2.82 Å), respectively. Through these results, it was confirmed that the amino acids of SARS CoV-2 3CLpro bound to flavonoids are similar to those that hydrogen bond with synthetic compounds in previous study [25].

3.4. Molecular dynamics analysis of the potential inhibitor with SARS-CoV-2 3CLpro

Until now, the binding method of enzyme and inhibitor were determined experimentally using crystal structures [26]. In an enzymatic reaction, inhibitors retain their binding to an enzyme in a fluid state [27]. This can be implemented virtually using molecular dynamics simulations with explicit water molecules. Therefore, this study performed a molecular dynamics analysis (Gromacs version 4.6.5 program) to investigate the binding of methoxyl flavonoids and SARS- CoV-2 3CLpro. For the virtual experiment, potential inhibitor **3** was used. The results were visually confirmed as snapshots at a 3 ns intervals (Fig. 4A). Inhibitor **3** was fitted with SARS-CoV-2 3CLpro during simulation with ~9 × 10^5 kJ/mol potential energy (Fig. 4B). Protein-based root-mean-square deviation (RMSD) and root-mean square-fluctuations (RMSF) confirmed a value within 0.4 nm (Fig. 4C and D). Inhibitor

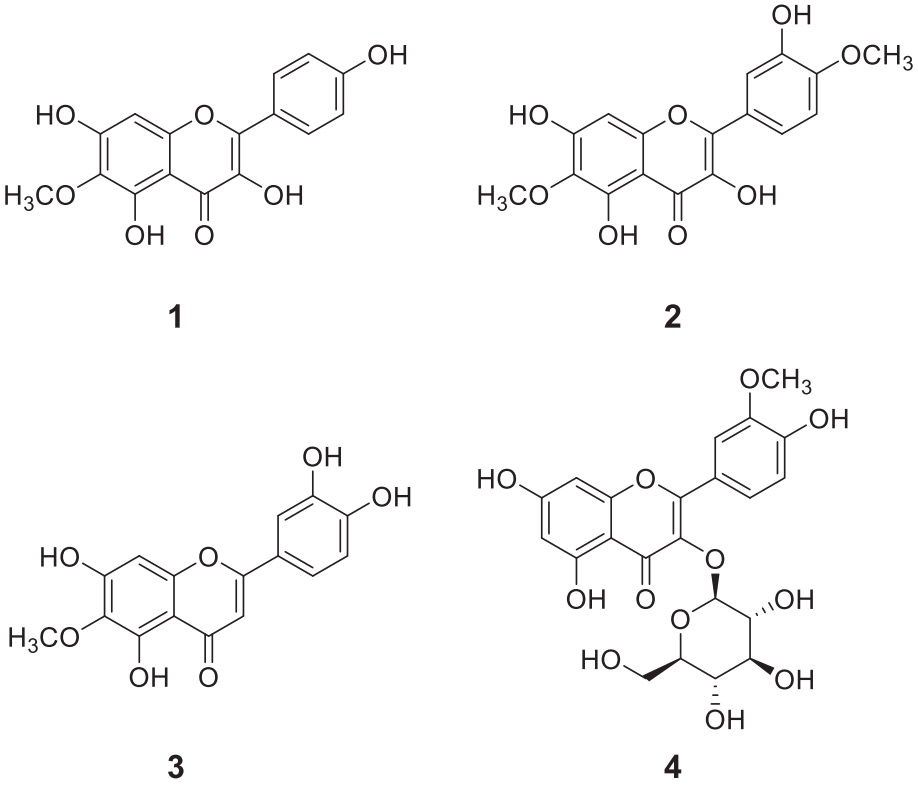

Fig. 1. The structure of isolated compounds **1**–**4** from *Inula japonica*. (**1**: hispidulin, **2**: patuletin, **3**: nepetin, **4**: isorhametin-3-*O*-glucoside.)

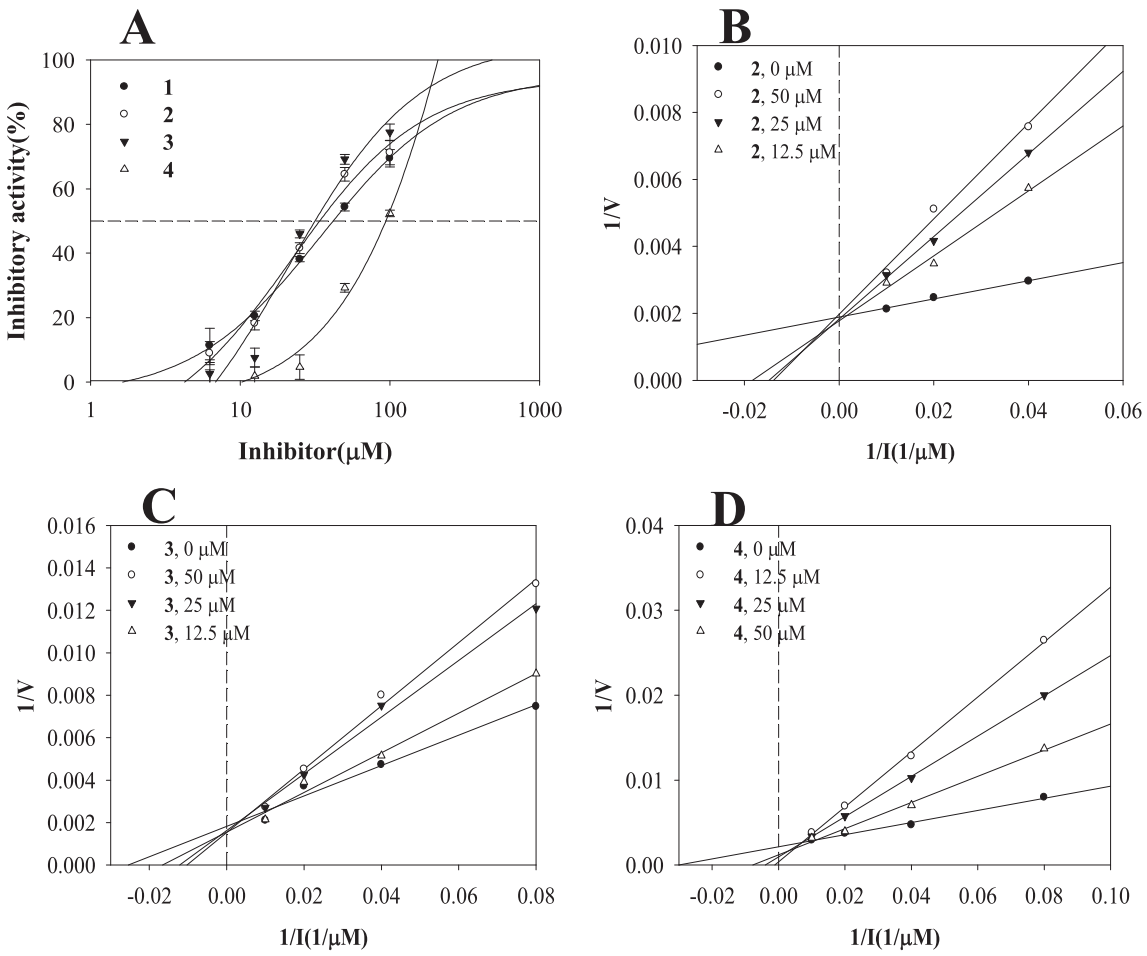

Fig. 2. The inhibitory activity of compounds **1**–**4** on 3CLpro (A). Lineweaver-Burk plot were constructed from the inhibition of 3CLpro by inhibitors **1**–**3** (B–D).

Table 1
The inhibitory activity of isolated compounds **1**–**4** from *I. japonica* on 3CLpro.

	IC_{50} (μM)[a]	Binding type
1	42.0 ± 1.7	Competitive
2	34.0 ± 0.5	Competitive
3	31.7 ± 1.1	Competitive
4	94.1 ± 2.5	–

[a] All compounds examined in a set of triplicated experiment.

Table 2
The hydrogen bonds interactions and Autodock score between 3CLpro and inhibitor.

Inhibitor	Hydrogen bonds (Å)	Autodock score (kcal/mol)
1	His164 (2.92), Glu166 (2.90), Arg188 (2.57), Thr190 (3.13), Gln192 (2.74)	−6.97
2	Glu166 (2.60), Arg188 (2.58), Gln189 (2.82), Thr190 (2.98), Gln192 (2.73)	−7.2
3	Cys145 (2.85), His164 (2.82), Arg188 (3.03), Thr190 (2.45, 2.91, 2.93), Gln192 (2.82)	−7.17

3 maintained 0–6 hydrogen bonds with 3CLpro residues for 30 ns with key amino acids (Fig. 4E). In particular, three key amino acids, Glu140, Leu141, and His172, mainly participate in hydrogen bonding during simulation between the inhibitor and enzyme (Fig. 4F and Table S1). The three amino acids maintained a distance of 0.4 nm or more to inhibitor **3** for 5000 ps, and then maintained a continuous proximity within a distance of ~0.35 nm (Fig. 4G and H).

3.5. Plaque formation assay

Three compounds (**1**–**3**) showed the inhibitory activity against SARS-CoV-2 3CLpro, and plaque formation assay were used to evaluate the inhibitory activity against coronavirus replication. Beta-coronavirus family contains SARS-CoV, SARS-CoV-2, MERS-CoV and HCoV-OC43 [28]. Previous sequence analysis study showed that SARS-CoV-2 3CLpro shares high similarity with HCoV-OC43 3CLpro [29]. Due to the strict regulation, HCoV-OC43 was used to examine the coronavirus replication as a surrogate. RD cells were treated with each compound and infected with the indicated dilution of media containing HCoV-OC43 coronavirus. While mock and compound **4** showed the similar number of plaque formation, three compounds **1**–**3** treatment decreased the number of plaques (Fig. 5). The inhibitors **1**–**4** showed an antiviral effect of 2.0×10^5, 1.8×10^5, 1.3×10^5, and 2.45×10^5 PFU value compared to 2.5×10^5 PFU of Mock, respectively. These results indicated that three compounds (**1**–**3**) can inhibit the coronavirus replication as well as SAR- CoV-2 3CLpro activity.

4. Discussion and conclusion

3CLpro cleaves polypeptides in the early stages of SARS-CoV-2 proliferation [12–14]. The recent development of the antiviral agent Paxlovid (nirmatrelvir and ritonavir tablets) has highlighted that inhibition of SARS-CoV-2 3CLpro proteolysis as an important factor in the development of SARS-CoV-2 therapeutics [30]. Natural products have been a

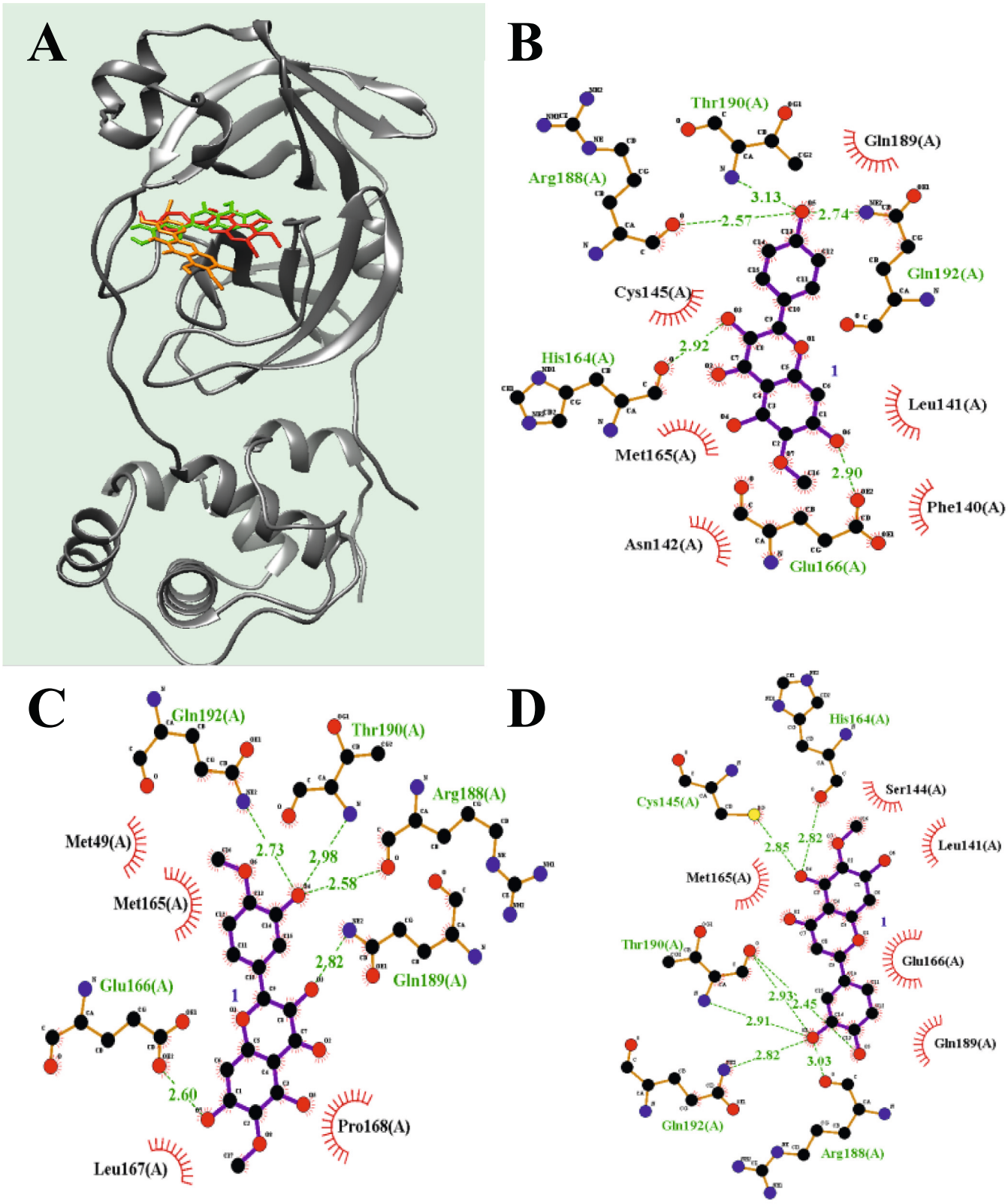

Fig. 3. The best docking position of compounds **1–3** (red, orange, and green) (A). The green dot line represents hydrogen bonds of inhibitor with amino acids of 3CLpro (B–D).

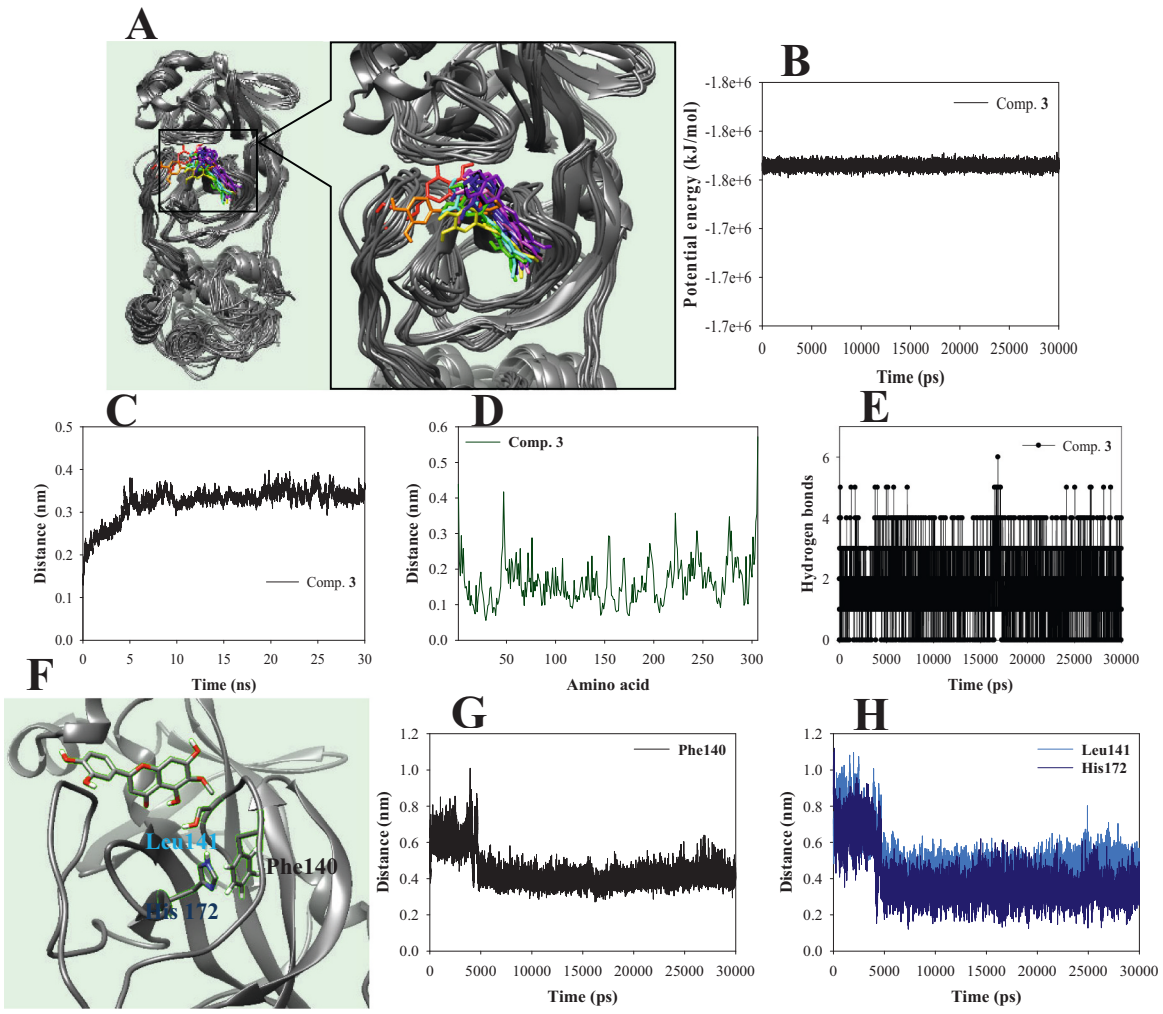

Fig. 4. The superpositions of 3CLpro with inhibitor **3** for the simulation time (red: 0 ns, orange: 3 ns, yellow: 6 ns, green: 9 ns, cyan: 12 ns, blue: 15 ns, conflower blue: 18 ns, purple: 21 ns, hot pink: 24 ns, magenta:27 ns, black: 30 ns) (A), The RMSD (B), RMSF (C), potential energy (D), and hydrogen bond numbers (E) of the simulation calculated during 30 ns. The distance of key residues with inhibitor **3** (F–H).

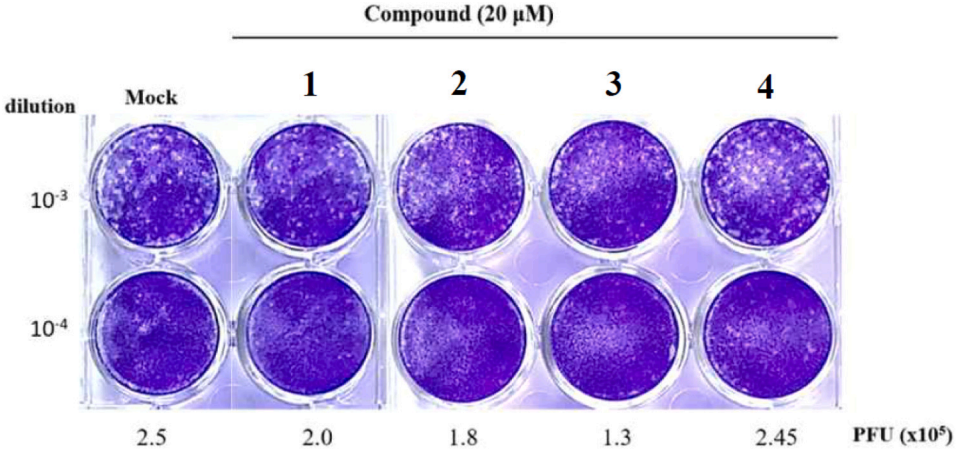

Fig. 5. Reduction of plaque numbers by the treatment of compounds **1**–**4**. RD cells were infected with HCoV-OC43 virus and treated with either mock or the indicated compound. To visualize the formation of plaques, the cells were stained with crystal violet. Calculated PFU were shown in the bottom.

source of medicine for thousands of years, and many of the drugs currently prescribed are derived from natural products [31]. They exhibit tremendous structural and chemical diversity, and approximately 40 % of chemical scaffolds found in natural products are absent in the medicinal chemistry repertoire [32]. Therefore, phytochemicals derived from medicinal plants with activity against targets associated with SARS-CoV infection may provide valuable leads for drug development against novel SARS-CoV-2. Recently, studies have been

conducted to develop SARS-CoV-2 3CLpro inhibitors from natural plants [33]. Some flavonoid derivatives, which are representative natural compounds, have an excellent effect on SARS-CoV-2 3CLpro [34]. We discovered four methoxyl flavonoids (hispidulin, patuletin, nepetin, and andisorhametin-3-*O*-glucoside) during our compositional study of the *I. britannica* flower. Except for the flavonoid glycoside **4**, three methoxyl flavonoids (**1**–**3**), which acted as competitive inhibitors, showed similar SARS-CoV2 3CLpro inhibitory effects, with IC_{50} values of 41.6 ± 2.5, 35.9 ± 0.9, and 32.8 ± 1.2 μM, respectively. Molecular docking showed a slight difference compared with SARS-CoV-2 3CLpro inhibition, but showed a similar trend to their inhibitory activity of HCoV-OC43 proliferation. In particular, the amino acids participating in hydrogen bonding in the molecular docking and molecular dynamics were significantly different. The reason for this is that docking of a ligand in a rigid SARS-CoV-2 3CLpro forms a bond with a restricted amino residue, but the amino acid residue freely binds to ligand when it is mobile. Molecular dynamic study found that Phe140, Leu141, and His172 maintained a hydrogen bond distance to the ligand after 5 ns. This fact identified three key amino acids that bind the ligand in the inhibitor **3**–SARS-CoV-2 3CLpro complex. Finally, the methoxyl flavonoid inhibitors **1**–**4** showed inhibitory effects against HCoV-OC43 coronavirus proliferation in the order of **3** > **2** > **1** > **4**.

In our study, four methoxyl flavonoids (**1**–**4**) isolated from *I. britannica* flower were identified. Of them, **1**–**3** were revealed to suppress the catalytic reaction of SARS-CoV-2 3CLpro as competitive mode. Molecular docking proved that they were stably docked to active site of SARS-CoV-2 3CLpro. The strong inhibitor **3** was familiar with Phe140, Leu141, and His172 among amino acids in that through molecular dynamics. Finally, inhibitors **1**–**3** had an inhibitory effect on HCoV-OC43 coronavirus proliferation at 20 μM.

Conflicts of interest

The authors declare that there is no conflict of interest.

Data availability

No data was used for the research described in the article.

Acknowledgement

This work was supported by the cooperative Research Program (PJ01708101) of Rural Development Administration, Republic of Korea.

Appendix A. Supplementary data

Supplementary data to this article can be found online at https://doi.org/10.1016/j.ijbiomac.2022.10.008.

References

[1] G. Fontana, M. Bruno, F. Senatore, C. Formisano, Volatile constituents of aerial parts of two mediterranean species of Inula: Inula crithmoides L. and I. verbascifolia (Willd.) Hausskn. (Asteraceae), Nat. Prod. Res. 28 (2014) 984–993.
[2] N.S. Bai, Z. Zhou, N.Q. Zhu, L. Zhang, Z. Quan, K. He, Q.Y. Zheng, C.T. Ho, Antioxidative flavonoids from the flower of Inula britannica, J. Food Lipids 12 (2005) 141–149.
[3] Y.M. Zhao, M.L. Zhang, Q.W. Shi, H. Kiyota, Chemical constituents of plants from the genus inula, Chem. Biodivers 3 (2006) 371–384.
[4] A.L. Khan, J. Hussain, M. Hamayun, S.A. Gilani, S. Ahmad, G. Rehman, Y.H. Kim, S. M. Kang, I.J. Lee, Secondary metabolites from Inula britannica L. And their biological activities, Molecules 15 (2010) 1562–1577.
[5] S.A. Tang, H. Zhu, N. Qin, J.Y. Zhou, E. Lee, D.X. Kong, M.H. Jin, H.Q. Duan, Anti-inflammatory terpenes from flowers of Inula japonica, Planta Med. 80 (2014) 583–589.
[6] N.-K. Lee, J.-H. Lee, Y. Lee, S. Ahn, S. Eom, H.-D. Paik, Antimicrobial effect of Inula britannica flower extract against Methicillin-resistant Staphylococcus aureus, Korean J. Microbiol. Biotechnol. 41 (2013) 335–340.
[7] Q.H. Song, T. Kobayashi, K. Iijima, T. Hong, J.C. Cyong, Hepatoprotective effects of Inula britannica on hepatic injury in mice, Phytother. Res. 14 (2000) 180–186.
[8] T. Kobayashi, Q.H. Song, T. Hong, H. Kitamura, J.C. Cyong, Preventative effects of the flowers of Inula britannica on autoimmune diabetes in C57BL/KsJ mice induced by multiple low doses of streptozotocin, Phytother. Res. 16 (2002) 377–382.
[9] J.J. Shan, M. Yang, J.W. Ren, Anti-diabetic and hypolipidemic effects of aqueous-extract from the flower of Inula japonica in alloxan-induced diabetic mice, Biol. Pharm. Bull. 29 (2006) 455–459.
[10] C.M. Wang, Z.J. Jia, R.L. Zheng, The effect of 17 sesquiterpenes on cell viability and telomerase activity in the human ovarian cancer cell line HO-8910, Planta Med. 73 (2007) 180–184.
[11] H.Z. Jin, D. Lee, J.H. Lee, K. Lee, Y.S. Hong, D.H. Choung, Y.H. Kim, J.J. Lee, New sesquiterpene dimers from Inula britannica inhibit NF-kappa B activation and NO and TNF-alpha production in LPS-stimulated RAW264.7 cells, Planta Med. 72 (2006) 40–45.
[12] A.M. Shaqra, S.N. Zvornicanin, Q.U.J. Huang, G.J. Lockbaum, M. Knapp, L. Tandeske, D.T. Bakan, J. Flynn, D.N.A. Bolon, S. Moquin, D. Dovala, N. K. Yilmaz, C.A. Schiffer, Defining the substrate envelope of SARS-CoV-2 main protease to predict and avoid drug resistance, Nat. Commun. 13 (2022) 3556.
[13] R. Wang, Q. Hu, H. Wang, G. Zhu, M. Wang, Q. Zhang, Y. Zhao, C. Li, Y. Zhang, G. Ge, H. Chen, L. Chen, Identification of vitamin K3 and its analogues as covalent inhibitors of SARS-CoV-2 3CLpro, Int. J. Biol. Macromol. 183 (2021) 182–192.
[14] H.-X. Su, S. Yao, W.-F. Zhao, M.-J. Li, J. Liu, W.-J. Shang, H. Xie, C.-Q. Ke, H.-C. Hu, M.-N. Gao, K.-Q. Yu, H. Liu, J.-S. Shen, W. Tang, L.-K. Zhang, G.-F. Xiao, L. Ni, D.-W. Wang, J.-P. Zuo, H.-I. Jiang, F. Bai, Y. Wu, Y. Ye, Y.-C. Xu, Anti-SARS-CoV-2 activities in vitro of Shuanghuanglian preparations and bioactive ingredients, Acta Pharm. Sin. 41 (2020) 1167–1177.
[15] P. V'kovski, A. Kratzel, S. Steiner, H. Stalder, V. Thiel, Coronavirus biology and replication: inplications for SARS-CoV-2, Nat. Rev. Microbiol. 19 (2021) 155–170.
[16] Q. Hu, Y. Xiong, G.-H. Zhu, Y.-N. Zhang, Y.-W. Zhang, P. Huang, G.-B. Ge, The SARS-CoV-2 main protease(Mpro): structure, function, and emerging therapies for COVID-19, MedComm 3 (2022), e151.
[17] A. Narayanan, M. Narwal, S.A. Majowicz, C. Varricchio, S.A. Toner, C. Ballatore, A. Brancale, K.S. Murakami, J. Jose, Commun. Biol. 5 (2022) 169.
[18] Y. Xiong, G.-H. Zhu, H.-N. Wang, Q. Hu, L.-L. Chen, X.-Q. Guan, H.-L. Li, H.-Z. Chen, H. Tang, G.-B. Ge, Discovery of naturally occurring inhibitors against SARS-CoV-2 3CLpro from Ginkgo biloba leaves via large-scale screening, Fitoterapia 152 (2021), 104909.
[19] Y. Xiong, G.-H. Zhu, Y.-N. Zhang, Q. Hu, H.-N. Wang, H.-N. Yu, X.-Y. Qin, X.-Q. Guan, Y.-W. Xiang, H. Tang, G.-B. Ge, Flavonoids in Ampelopsis grossedentata as covalent inhibitors of SARS-CoV-2 3CLpro: inhibition potentials, covalent binding sites and inhibitory mechanisms, Inter. J. Biol. Macromol. 187 (2021) 976–987.
[20] P.K. Tripathi, S. Upadhyay, M. Singh, S. Raghavendhar, M. Bhardwaj, P. Sharma, A.K. Patel, Screening and evaluation of approved drugs as inhibitors of main protease of SARS-CoV-2, Int. J. Biol. Macromol. 164 (2020) 2622–2631.
[21] M. Hoshi, S. Shiino, A. Gomi, K. Sakata, S. Konno, Y. Hayashi, M. Kojima, In silico design of inhibitor against SARS-CoV-2 protease by docking simulation and ADMET prediction, Bioimages 29 (2021) 11–21.
[22] J.H. Kim, Y.D. Jo, H.-Y. Kim, B.-R. Kim, B. Nam, In vitro and in silico insights into sEH inhibitors with amide-scaffold from the leaves of Capsicum chinense jacq, Comput. Struct. Biotechnol. J. 16 (2018) 404–411.
[23] W. Zeng, Quesheng, Q. Zhang, H. Liang, Flavonoids from Artemisia gmelinii Web. ex Stechm, J. Chin. Pharm. Sci. 23 (2014) 496–499.
[24] A.M. El-Hawiet, S.M. Toaima, A.M. Asaad, M.M. Radwan, N.A. El-Sebakhy, Chemical constituents from Astragalus annularis forssk. And A. Trimestris LFabaceae, Rev. Bras. Farmacogn. 20 (2010) 860–865.
[25] M. Jukič, D. Janežič, U. Bren, Ensemble docking coupled to linear interaction energy calculations for identification of coronavirus main protease (3CLpro) non-covalent small-molecule inhibitors, Molecules 25 (2020) 5808.
[26] J. Lee, L.J. Worrall, M.V. Vuckovic, F.I. Rosell, F. Gentile, A.-T. Ton, N.A. Caveney, F. Ban, A. Cherkasov, M. Paetzel, N.C.J. Strynadka, Crystallographic structure of wild-type SARS-CoV-2 main protease acyl-enzyme intermediate with physiological C-terminal autoprocessing site, Nat. Commun. 11 (2020) 5877.
[27] K.A. Johnson, Role of induced fit in enzyme specificity: a molecular forward/reverse switch, J. Biol. Chem. 283 (2008) 26297–26301.
[28] M. Jang, R. Park, Y.-I. Park, Y.-E. Cha, A. Yamamoto, J.I. Lee, J. Park, EGCG, a green tea polyphenol, inhibits human coronavirus replication in vitro, Biochem. Biophys. Res. Commun. 547 (2021) 23–28.
[29] C.B. Jackson, M. Farzan, B. Chem, H. Choe, Mechanisms of SARS-CoV-2 entry into cells, Nat. Rev. Mol. Cell Biol. 23 (2022) 3–20.
[30] S.E. Greasley, S. Noell, O. Plotnikova, R. Ferre, W. Liu, B. Bolano, K. Fennel, J. Nicki, T. Craig, Y. Zhu, A.E. Stewart, C.M. Steppan, Structural basis for the in vitro efficacy of nirmatrelvir against SARS-CoV-2 variants, J. Biol. Chem. 298 (2022), 101972.
[31] A. Harvey, The role of natural products in drug discovery and development in the new millennium, IDrugs 13 (2010) 70–72.
[32] M.-L. Lee, G. Schneider, Scaffold architecture and pharmacophoric properties of natural products and trade drugs: application in the design of natural product-based combinatorial libraries, J. Comb. Chem. 3 (2001) 284–289.
[33] D. Latha, D. Hrishikesh, G. Shiban, C. Chandrashekar, B.R. Bharath, In silico, in vitro screening of plant extracts for anti-SARS-CoV-2 activity and evaluation of their acute and sub-acute toxicity, Phytomed. Plus 2 (2022), 100233.
[34] S. Jo, S. Kim, D.Y. Kim, M.-S. Kim, D.H. Shin, Flavonoids with inhibitory activity against SARS-CoV-2 3CLpro, J. Enzyme Inhib. Med. Chem. 35 (2020) 1539–1544.